Ranging in a Dense Multipath Environment Using an UWB Radio Link

Joon-Yong Lee and Robert A. Scholtz, *Life Fellow, IEEE*

***Abstract*—A time-of-arrival (ToA)-based ranging scheme using an ultra-wideband (UWB) radio link is proposed. This ranging scheme implements a search algorithm for the detection of a direct path signal in the presence of dense multipath, utilizing generalized maximum-likelihood (GML) estimation. Models for critical parameters in the algorithm are based on statistical analysis of propagation data and the algorithm is tested on another independent set of propagation measurements. The proposed UWB ranging system uses a correlator and a parallel sampler with a high-speed measurement capability in each transceiver to accomplish two-way ranging between them in the absence of a common clock.**

***Index Terms*—Delay estimation, distance measurement, multipath channels, ultra-wideband (UWB).**

I. Introduction

THE FINE time resolution of ultra-wideband (UWB) signals enables potential applications in high-resolution ranging. The novel aspect of UWB ranging is the fact that the multipath time-spread in many channels of interest is often 100 to 1000 times the inherent time resolution of the UWB signal detected in a matched-filter receiver. Detection of the direct path signal in the presence of dense multipath, which determines ranging quality, becomes a different kind of problem in this case. Multipath resolution techniques in narrowband systems have been well developed [8], [9]. Win and Scholtz [2] introduced a maximum-likelihood (ML) detector for multipath in UWB propagation measurements and Cramer *et al.* [4]–[6] used the CLEAN algorithm to develop a UWB channel model involving angle-of-arrival (AoA), as well as time-of-arrival (ToA).

This paper introduces a ToA measurement algorithm utilizing generalized maximum-likelihood (GML) estimation for the detection of the direct-path signal. Multipath delay and amplitude parameters appearing in this algorithm are modeled statistically from propagation data and the algorithm is tested on an independent set of propagation measurements. Probabilistic analysis of different kinds of errors using these statistical models provides a way of determining the thresholds used in the ToA algorithm, as well as estimating the algorithm's performance. We conclude by presenting the schematic design of an UWB ranging system with a high-speed measurement capability and a two-way ranging technique that utilizes this algorithm.

Manuscript received December 14, 2001. This work was supported by the Office of Naval Research under Contract N00014-00-0221.

J.-Y. Lee was with the Ultra-Wideband Radio Laboratory, University of Southern California, Los Angeles, CA 90089-2560 USA. He is now with School of Computer Science & Electrical Engineering, Handong Global University, Pohang, Korea (e-mail: joonlee@handong.edu).

R. A. Scholtz is with the Communications Sciences Institute, Department of Electrical Engineering–Systems, University of Southern California, Los Angeles, CA 90089-2565 USA (email: scholtz@usc.edu).

Digital Object Identifier 10.1109/JSAC.2002.805060

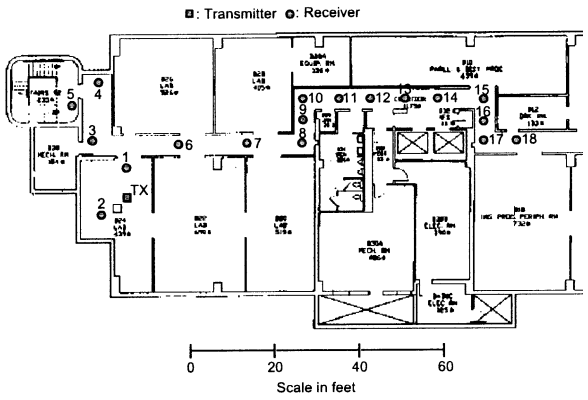

Fig. 1. Basement floor plan of the building where the experiments were conducted. Interior walls are metal stud and dry wall construction. Circular marks stand for the locations of the receiving antenna and the rectangular mark indicates the transmitting antenna's location.

II. Propagation Measurement

A set of indoor propagation measurements was conducted at the University of Southern California to test the ToA algorithm presented in the next section. Pulses with a subnanosecond width were transmitted with one microsecond spacing and measured with a digital sampling scope. The antennas were vertically polarized diamond dipoles [10], approximately 5 ft above the floor. The sampling rate of the measured signal is 20.5 GHz. Sampled waveforms were averaged over 512 sweeps to acquire a higher signal-to-noise ratio (SNR).

Fig. 1 is the floor plan of the building where the measurements were taken. Signals were measured at 18 different locations while the transmitter was fixed in the laboratory. At location 1, the signal was measured with a visually clear line-of-sight (LoS) and used to calibrate the arrival time of the direct path signal. The other 17 signals were measured with a blocked LoS. At locations 16–18, the LoS path was blocked by an elevator (a metallic structure), so the direct path signal could not be measured while multipath could be observed.

Fig. 2 shows the samples of signals taken at location 1, 4, and 14, respectively. Notice that the signals shown in the second and the third plot have stronger multipath components than the direct path signal. In these cases, if a ranging system synchronizes with the strongest signal component for the purpose of range estimation, a large-scale error will occur. The presence of reflected signals that are stronger than the direct path signal makes ranging to the full capabilities of UWB signals challenging.

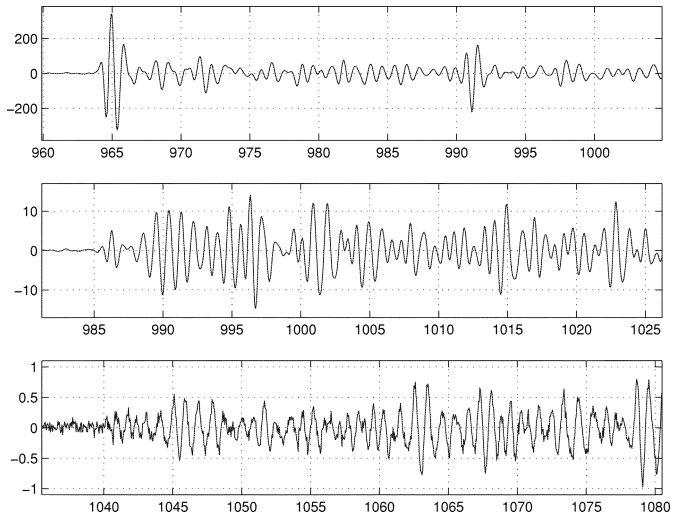

Fig. 2. Measured signals at location 1, 4, and 14. The vertical axis indicates signal strength in millivolts. The vertical scales of each plot are different, indicating differences in channel attenuation. The signal shown in the first plot was measured with a clear LoS and the others were measured in the presence of LoS blockages.

III. Detection of Direct Path Signals

In this paper, the direct path signal is assumed to be the earliest arrival at the receiver. When the straight-line path from transmitter to receiver is in fact a viable propagation path, ToA estimation of the direct path signal is useful for ranging. As shown in the signals of Fig. 2, the direct path signal is not always the strongest in the presence of a visual LoS blockage. The ToA algorithm in this section does not assume that the direct path always supplies the strongest response.

A. Signal Representation

When a single pulse is transmitted, the received signal is composed of direct path signal, reflected signals, noise, and interference [1]. So the received signal $r_{\rm m}(t)$ can be represented by

$$r_{\rm m}(t) = a_{\rm d}s(t-\tau_{\rm d}) + \sum_{n=1}^{L} a_n s(t-\tau_n) + n_{\rm m}(t) \qquad (1)$$

where $\tau_{\rm d} < \tau_1 < \tau_2 < \cdots < \tau_L$. The parameters $\tau_{\rm d}$ and $a_{\rm d}$ are the arrival time and strength of the direct path signal, respectively, and τ_n and a_n are those of the nth reflected component. The waveform $s(t)$ denotes the canonical single-path signal, used as a correlator template, with a width of $T_{\rm p}$ seconds. The number of multipath signals L is unknown *a priori*. The noise $n_{\rm m}(t)$ is assumed to be additive white Gaussian, and interference is assumed to be zero.

Let $\tau_{\rm peak}$ and $a_{\rm peak}$ be the arrival time and amplitude of the strongest path and assume these have been determined by correlation. Then, $r_{\rm s}(t)$, a normalized and shifted version of $r_{\rm m}(t)$, can be represented by

$$\begin{aligned} r_{\rm s}(t) &= \frac{1}{|a_{\rm peak}|}\, r_{\rm m}(t+\tau_{\rm peak}) \\ &= \rho_{\rm d} s(t+\delta) + \sum_{n}^{L} \alpha_n s(t+\beta_n) + n_{\rm s}(t) \qquad (2) \\ &= \rho_{\rm d} s(t+\delta) + \sum_{\beta_n \geq 0} \alpha_n s(t+\beta_n) \\ &\quad + \sum_{\beta_n < 0} \alpha_n s(t+\beta_n) + n_{\rm s}(t) \qquad (3) \end{aligned}$$

where

$$\begin{cases} \delta = \tau_{\rm peak} - \tau_{\rm d}, & \delta \geq 0 \\ \rho_{\rm d} = a_{\rm d}/|a_{\rm d}|, & -1 \leq \rho_{\rm d} \leq 1 \\ \beta_n = \tau_{\rm peak} - \tau_n, & \delta > \beta_1 > \beta_2 > \cdots > \beta_L \\ \alpha_n = a_n/|a_{\rm d}|, & -1 \leq \alpha_n \leq 1,\ \forall n \leq L. \end{cases} \qquad (4)$$

The noise $n_{\rm s}(t)$ being a time-shifted version of $n_{\rm m}(t)$, is a white Gaussian noise signal. The third term in (3) represents the multipath components which arrive later than the peak path. To simplify the problem, let us restrict our observation to the portion of the signal prior to and including the arrival of the strongest path by truncating $r_{\rm s}(t)$. Let us define $r(t)$ as

$$\begin{aligned} r(t) &= r_{\rm s}(t), \qquad t \leq \frac{T_{\rm p}}{2} \\ &= \rho_{\rm d} s(t+\delta) + \sum_{\beta_k \geq 0} \alpha_k s(t+\beta_k) + n(t), \qquad t \leq \frac{T_{\rm p}}{2} \\ &= \rho_{\rm d} s(t+\delta) + \sum_{k=1}^{M} \alpha_k s(t+\beta_k) + n(t), \qquad t \leq \frac{T_{\rm p}}{2} \end{aligned} \qquad (5)$$

where M is the number of signal components that arrived earlier than the peak component. If M is equal to zero, then $\delta = 0$, $\rho_{\rm d} = \pm 1$, and the second term in (5) is ignored. The noise $n(t)$ is white Gaussian noise [truncated to the interval $(-\infty, T_{\rm p}/2)$], whose correlation function is represented by

$$R_{\rm N}(\tau) = \sigma_{\rm A}^2 \cdot \delta_{\rm D}(\tau). \qquad (6)$$

Assuming $r(t)$ is sampled, let us represent it as a vector of samples, namely

$$\underline{r} = \rho_{\rm d}\underline{s}_{\,\delta} + \sum_{k=1}^{M} \alpha_k \underline{s}_{\,\beta_k} + \underline{n} \qquad (7)$$

where $\underline{s}_{\,\beta}$ represents the vector of samples of $s(t+\beta)$ with a same length as $\underline{r}$. The noise vector $\underline{n}$ is a white Gaussian vector whose correlation matrix $R_{\rm N}$ is given by

$$R_{\rm N} = \sigma_{\rm N}^2 \cdot I \qquad (8)$$

I being an identity matrix.

B. ToA Measurement Algorithm Using GML Estimation

In (7), δ is the parameter to be estimated and $\rho_{\rm d}$, M, $\underline{\alpha}^M$, and $\underline{\beta}^M$ are nuisance parameters, where $\underline{\alpha}^M$ and $\underline{\beta}^M$ are defined as

$$\underline{\alpha}^M = (\alpha_1, \alpha_2, \ldots, \alpha_M) \qquad (9)$$

$$\underline{\beta}^M = (\beta_1, \beta_2, \ldots, \beta_M). \qquad (10)$$

GML estimation treats all of these unknown parameters as deterministic and estimates δ to be

$$\hat{\delta} = \arg\max_{\delta} \left[\max_{\rho_{\rm d},\, M,\, \underline{\alpha},\, \underline{\beta}} f\left(\underline{r}|\delta,\, \rho_{\rm d},\, M,\, \underline{\alpha}^M,\, \underline{\beta}^M\right) \right]. \qquad (11)$$

Because $\underline{n}$ is a white Gaussian vector, this is equivalent to

$$\hat{\delta} = \arg\min_{\delta} \left[\min_{\rho_{\rm d}, M, \underline{\alpha}, \underline{\beta}} \left\| \underline{r} - \rho_{\rm d} \underline{s}_{\delta} - \sum_{k=1}^{M} \alpha_k \underline{s}_{\beta_k} \right\|^2 \right]. \quad (12)$$

Using (12) to estimate δ is computation intensive because $2(M+1)$ unknown parameters are involved. To reduce computational complexity, an iterative nonlinear programming technique is employed, by which the unknown parameters are estimated in a sequential manner [2]. Specifically, the arrival time of each component signal is estimated individually while all other parameters are fixed.

Modification of the estimation criterion shown in (12) is done as follows. First, the duration of the search region for the time δ of arrival of the direct path signal is limited to prevent the probability of a false detection in the noise only portion of the observed signal from becoming too large. We define θ_δ as a limiting threshold on $\boldsymbol{\delta}$ so that the direct path signal is searched over the portion of $r(t)$ satisfying $t \geq -\theta_\delta$. Second, a stopping rule is used to terminate the search, because the value of the norm in (12) generally continues to decrease with increasing M. The stopping rule consists of applying a threshold on the relative path strength ρ which is defined as

$$\rho = |\rho_{\rm d}|. \quad (13)$$

The iterative search process stops when no more paths satisfying $\rho \geq \theta_\rho$ are detected in the search region, where θ_ρ is the threshold of ρ. Third, we skip the estimation of some nuisance parameters by ignoring the multipath components that arrive later than already detected paths. By doing this, we can speed up the search process. Following is a brief description of the ToA algorithm.

1) Let $n = 1$, $\omega_1 = 0$, and $\mu_{11} = 1$.
2) Increase n by 1.
3) Find ω_n which satisfies

$$\omega_n = \arg \max_{\omega_{n-1} < \omega < \theta_\delta} \left(\underline{r} - \sum_{i=1}^{n-1} \mu_{(n-1)i} \underline{s}_{\omega_i} \right)^{\rm t} \underline{s}_{\omega} \quad (14)$$

4) Find $(\mu_{n1}, \mu_{n2}, \ldots, \mu_{nn})$ such that

$$(\mu_{n1}, \mu_{n2}, \ldots, \mu_{nn}) = \arg \min_{\mu'_1, \ldots, \mu'_2} \left\| \underline{r} - \sum_{i=1}^{n} \mu'_i \underline{s}_{\omega_i} \right\|^2. \quad (15)$$

5) If $\mu_{nn} \geq \theta_\rho$, go to step 2. Otherwise, proceed to the next step.
6) δ is estimated as $\hat{\delta} = \omega_{n-1}$.

IV. Statistical Modeling of Ranging Parameters

The thresholds θ_δ and θ_ρ, which are used in the ToA algorithm have to be determined so that they satisfy a given performance criteria. One of the potential criteria is that the probability of error is minimized. For the purpose of error analysis, the parameters $\boldsymbol{\delta}$ and $\boldsymbol{\rho}$ which were defined in Section III-A were modeled statistically.

A set of propagation data taken by Win [3] in an office building was used for this modeling. The values of δs and

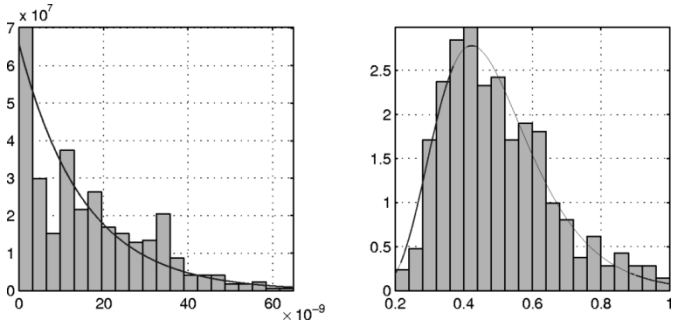

Fig. 3. Normalized histograms of (a) $\boldsymbol{\delta}$ and (b) $\boldsymbol{\rho}$ and approximation of marginal densities using curve-fitting.

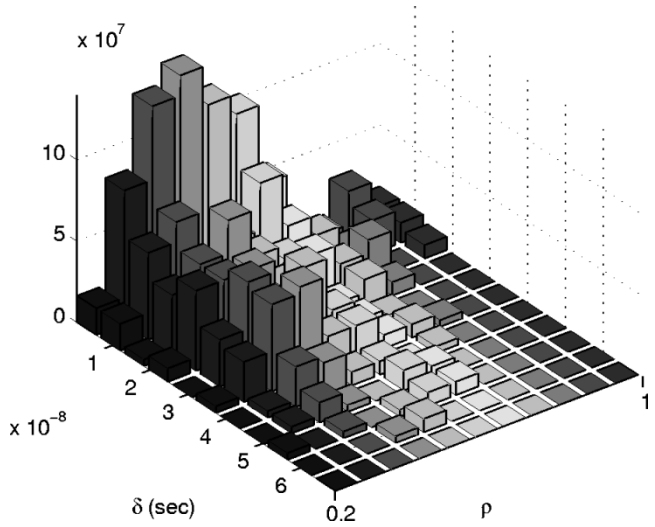

Fig. 4. Histogram of $\boldsymbol{\rho}$ and $\boldsymbol{\delta}$. Total volume was normalized to one.

ρs of 622 signals which were measured with a blocked LoS were extracted using the ToA algorithm. The values of θ_δ and θ_ρ used in this process were 70 ns and 0.2, respectively. Some large scale errors relative to the approximately known distance information were corrected by manually adjusting the thresholds. In 95 of 622 observed signals, the direct path signal was the strongest. So if we define P_0 as the probability that $\boldsymbol{\delta}$ is equal to zero, it can be modeled by

$$P_0 = \Pr(\boldsymbol{\delta} = 0) = \Pr(\boldsymbol{\rho} = 1) = 0.1527. \quad (16)$$

Fig. 3(a) and (b) are normalized histograms of $\boldsymbol{\delta}$ and $\boldsymbol{\rho}$ which were produced with 527 signals that have a stronger reflected path than the direct path. By curve fitting on this data, marginal densities of $\boldsymbol{\delta}$ and $\boldsymbol{\rho}$ can be modeled by

$$f_{\boldsymbol{\delta}}(\delta | \boldsymbol{\delta} \neq 0) = \frac{1}{\sigma_\delta} e^{-\delta/\sigma_\delta}, \qquad \delta > 0 \quad (17)$$

$$f_{\boldsymbol{\rho}}(\rho | \boldsymbol{\rho} \neq 1) = \frac{1}{\sqrt{2\pi} Q(-\mu_\rho/\sigma_\rho) \sigma_\rho \rho} e^{-(\ln \rho - \mu_\rho)^2 / 2\sigma_\rho^2} \qquad 0 < \rho < 1 \quad (18)$$

where $\sigma_\delta = 1.524 \times 10^{-8}$, $\sigma_\rho = 0.3220$, and $\mu_\rho = -0.7565$. The Q-function appearing in (18) is for normalization.

Independence between $\boldsymbol{\delta}$ and $\boldsymbol{\rho}$ was tested using a chi-squared test. Chi-squared test uses the contingency data set of categorical variables [13], [14]. Fig. 4 is the normalized histogram of δ

and ρ. Pearson's statistic χ^2 with 100 degrees of freedom, which was evaluated with the data set, is 117.2. According to the χ^2 distribution table, the critical value corresponding to a 10% significance level and 100 degrees of freedom is 118.5, which is greater than the value evaluated with data. So we can accept the hypothesis of independence between $\boldsymbol{\delta}$ and $\boldsymbol{\rho}$ with a 10% significance level. Based on this result, the joint density of $\boldsymbol{\delta}$ and $\boldsymbol{\rho}$ can be modeled by

$$\begin{aligned} &f_{\boldsymbol{\delta\rho}}(\delta,\, \rho|\boldsymbol{\delta}\neq 0,\, \boldsymbol{\rho}\neq 1) \\ &\quad = f_{\boldsymbol{\delta}}(\delta|\boldsymbol{\delta}\neq 0)\cdot f_{\boldsymbol{\rho}}(\rho|\boldsymbol{\rho}\neq 1) \\ &\quad = \frac{1}{\sqrt{2\pi}Q(-\mu_\rho/\sigma_\rho)\sigma_\delta\sigma_\rho\rho}\exp\left\{-\left[\frac{\delta}{\sigma_\delta}+\frac{(\ln\rho-\mu_\rho)^2}{2\sigma_\rho^2}\right]\right\} \end{aligned} \tag{19}$$

where $\delta > 0$ and $0 < \rho < 1$.

V. Error Analysis

Range estimation error can result from two major sources. One is ToA estimation error, and the other is any unknown propagation delay in a LoS blockage structure, which is difficult to estimate without a more thorough knowledge of the blockage. In this section, errors in ToA estimation of the direct path signal are analyzed probabilistically.

We can classify ToA errors into two categories. One is early false alarms which occur when a false detection in the noise-only portion of the signal is regarded as that of direct path signal. The other is a missed direct-path error, which occurs when the actual direct path signal is missed and a multipath signal is falsely declared to be direct path signal.

A. Probability of an Early False Alarm

An early false alarm probability $P_{\rm FA}$ can be expressed as

$$\begin{aligned} P_{\rm FA} &= \Pr\left\{\sup_{\beta\in[-\theta_\delta,\, -\boldsymbol{\delta}-T_{\rm p})}\frac{|\underline{n}^t\underline{s}_\beta|}{\|\underline{s}_0\|^2}>\theta_\rho \text{ and } \boldsymbol{\delta}\le\theta_\delta-T_{\rm p}\right\} \\ &= \int_0^{\theta_\delta}\Pr\left\{\sup_{\beta\in[-\theta_\delta,\, -\delta-T_{\rm p})}\frac{|\underline{n}^t\underline{s}_\beta|}{\|\underline{s}_0\|^2}>\theta_\rho\right\} \\ &\quad\cdot f_{\boldsymbol{\delta}}(\delta|\boldsymbol{\delta}\neq 0)\,d\delta\cdot(1-P_0) \\ &\quad+\Pr\left\{\sup_{\beta\in[-\theta_\delta,\, -T_{\rm p})}\frac{|\underline{n}^t\underline{s}_\beta|}{\|\underline{s}_0\|^2}>\theta_\rho\right\}\cdot P_0 \\ &= \int_0^{\theta_\delta}\Pr\left\{\sup_{\beta\in[-\theta_\delta,\, -\delta-T_{\rm p})}\frac{|\underline{w}^t\underline{s}_\beta|}{\|\underline{s}_0\|^2}>\frac{\theta_\rho}{\sigma_{\rm N}}\right\} \\ &\quad\cdot f_{\boldsymbol{\delta}}(\delta|\boldsymbol{\delta}\neq 0)d\delta\cdot(1-P_0) \\ &\quad+\Pr\left\{\sup_{\beta\in[-\theta_\delta,\, -T_{\rm p})}\frac{|\underline{w}^t\underline{s}_\beta|}{\|\underline{s}_0\|^2}>\frac{\theta_\rho}{\sigma_{\rm N}}\right\}\cdot P_0 \end{aligned} \tag{20}$$

where

$$\underline{w}=\frac{1}{\sigma_{\rm N}}\,\underline{n}. \tag{21}$$

Let us define the peak SNR as the ratio of the peak signal power to the noise power. This can be expressed as

$$\mathrm{SNR_p}=\frac{1}{\sigma_{\rm N}^2} \tag{22}$$

because the signal was normalized to its peak strength. Substituting (22) into (20)

$$\begin{aligned} P_{\rm FA} &= \int_0^{\theta_\delta}\Pr\left\{\sup_{\beta\in[-\theta_\delta,\, -\delta-T_{\rm p})}\frac{|\underline{w}^t\underline{s}_\beta|}{\|\underline{s}_0\|^2}>\theta_\rho\sqrt{\mathrm{SNR_p}}\right\} \\ &\quad\cdot f_{\boldsymbol{\delta}}(\delta|\boldsymbol{\delta}\neq 0)d\delta\cdot(1-P_0) \\ &\quad+\Pr\left\{\sup_{\beta\in[-\theta_\delta,\, -T_{\rm p})}\frac{|\underline{w}^t\underline{s}_\beta|}{\|\underline{s}_0\|^2}>\theta_\rho\sqrt{\mathrm{SNR_p}}\right\}\cdot P_0. \end{aligned} \tag{23}$$

Let us define γ and a random process $\boldsymbol{u}(\beta)$ as

$$\gamma=\theta_\rho\cdot\sqrt{\mathrm{SNR_p}} \tag{24}$$

$$\boldsymbol{u}(\beta)=\frac{|\underline{w}^t\underline{s}_\beta|}{\|\underline{s}_0\|^2}. \tag{25}$$

Substituting (24) and (25) into (23)

$$\begin{aligned} P_{\rm FA} &= \int_0^{\theta_\delta}\Pr\left\{\sup_{\beta\in[-\theta_\delta,\, -\delta-T_{\rm p})}\boldsymbol{u}(\beta)>\gamma\right\}f_{\boldsymbol{\delta}}(\delta|\boldsymbol{\delta}\neq 0)\,d\delta \\ &\quad\cdot(1-P_0)+\Pr\left\{\sup_{\beta\in[-\theta_\delta,\, -T_{\rm p})}\boldsymbol{u}(\beta)>\gamma\right\}\cdot P_0. \end{aligned} \tag{26}$$

$\Pr\{\sup_{\beta\in[-\theta_\delta,\, -\delta-T_{\rm p})}\boldsymbol{u}(\beta)>\gamma\}$ can be modeled as a high level crossing probability of a random process $\boldsymbol{u}(\beta)$ at a level γ in a given time period $[-\theta_\delta,\, -\delta-T_{\rm p})$. This probability can be approximated by [11]

$$\Pr\left\{\sup_{\beta\in[-\theta_\delta,\, -\delta-T_{\rm p})}\boldsymbol{u}(\beta)>\gamma\right\}\approx 1-e^{-(\theta_\delta-\delta-T_{\rm p})/E(\boldsymbol{\lambda})} \tag{27}$$

where $\boldsymbol{\lambda}$ represents the time between a down-crossing and the next adjacent up-crossing at a given level γ. The expected value of $\boldsymbol{\lambda}$ was simulated using a computer generated white Gaussian vector. The value of $\boldsymbol{\lambda}$ for a given γ was observed over 100 occurrences and averaged. By curve-fitting on the simulation result, $E(\boldsymbol{\lambda})$ can be modeled by

$$E(\boldsymbol{\lambda})=C\cdot e^{B\gamma} \tag{28}$$

where $B = 6.5757$ and $C = 1.375\times 10^{-11}$. Substituting (28) into (27)

$$\begin{aligned} &\Pr\left\{\sup_{\beta\in[-\theta_\delta,\, -\delta-T_{\rm p})}\boldsymbol{u}(\beta)>\gamma\right\} \\ &\qquad = 1-\exp\left[-\frac{(\theta_\delta-\delta-T_{\rm p})}{C}\,e^{-B\gamma}\right]. \end{aligned} \tag{29}$$

Substituting (17) and (29) into (26), we get

$$\begin{aligned} P_{\rm FA} &= 1-(1-P_0)\,\frac{\sigma_\delta e^{-(\theta_\delta-T_{\rm p})/\sigma_\delta}}{\sigma_\delta-Ce^{B\gamma}} \\ &\quad-\frac{P_0\sigma_\delta-Ce^{B\gamma}}{\sigma_\delta-Ce^{B\gamma}}\exp\left[-\frac{(\theta_\delta-T_{\rm p})}{C}\,e^{-B\gamma}\right]. \end{aligned} \tag{30}$$

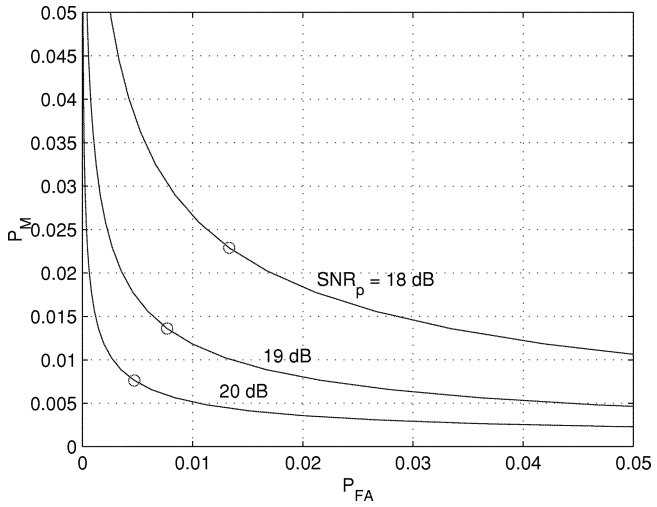

Fig. 5. Early false alarm probability versus probability of a missed direct path for different peak SNRs. $\theta_\delta = 100$ ns and θ_ρ was varied. At the circular mark on each curve, probability of error is minimized.

Substituting (24) into (30)

$$P_{\mathrm{FA}} = 1 - (1 - P_0)\,\frac{\sigma_\delta e^{-(\theta_\delta - T_{\mathrm{p}})/\sigma_\delta}}{\sigma_\delta - Ce^{B\theta_\rho\sqrt{\mathrm{SNR_p}}}} - \frac{P_0\sigma_\delta - Ce^{B\theta_\rho\sqrt{\mathrm{SNR_p}}}}{\sigma_\delta - Ce^{B\theta_\rho\sqrt{\mathrm{SNR_p}}}} \cdot \exp\left[-\frac{(\theta_\delta - T_{\mathrm{p}})}{C}\,e^{-B\theta_\rho\sqrt{\mathrm{SNR_p}}}\right]. \quad (31)$$

B. Probability of a Missed-Direct-Path Error

The probability P_{M} of a missed-direct-path error can be evaluated by computing

$$\begin{aligned} P_{\mathrm{M}} &= \Pr(\boldsymbol{\delta} > \theta_\delta \text{ or } \boldsymbol{\rho} < \theta_\rho) \\ &= 1 - \Pr(0 \le \boldsymbol{\delta} \le \theta_\delta \text{ and } \theta_\rho \le \boldsymbol{\rho} \le 1) \\ &= 1 - P_0 - (1 - P_0)\int_{\theta_\rho}^{1}\int_{0}^{\theta_\delta} f_{\boldsymbol{\delta\rho}}(\delta, \rho | \boldsymbol{\delta} \ne 0)\, d\delta\, d\rho. \end{aligned} \quad (32)$$

Substituting (19) into (32)

$$P_{\mathrm{M}} = (1 - P_0)\left[1 - \left(1 - e^{-\theta_\delta/\sigma_\delta}\right)\left(1 - \frac{Q\left(\frac{\ln\theta_\rho - \mu_\rho}{\sigma_\rho}\right)}{Q\left(\frac{-\mu_\rho}{\sigma_\rho}\right)}\right)\right]. \quad (33)$$

Fig. 5 is a plot of P_{FA} versus P_{M} for different values of peak SNR. The value of θ_δ was fixed at 100 ns and these two error probabilities were calculated for various θ_ρ. The circular mark on each curve represents the points where the sum of the two error probabilities is minimized.

VI. Test on Measured Data

Fig. 6 shows of test results of the ToA algorithm on the signals measured at location 9 and 13. In each example, the upper plot is the measured waveform and the lower one shows the reconstructed signal with the paths detected in the ToA algorithm. The value of θ_ρ was determined so that the total probability of error ($P_{\mathrm{FA}} + P_{\mathrm{M}}$) is minimized while θ_δ was fixed. The vertical line appearing in each plot indicates the expected arrival time of the direct-path signal in the presence of a clear LoS path, based on physical range measurements. We can observe a few nanoseconds of discrepancy between this line and signal frontend in both examples. This probably is caused by excessive propagation delay in the LoS blockage. This unknown delay makes it difficult to measure the true arrival time of direct path.

Fig. 7 shows the range estimation errors incurred in this test at the locations marked in Fig. 1. Notice that larger errors occurred

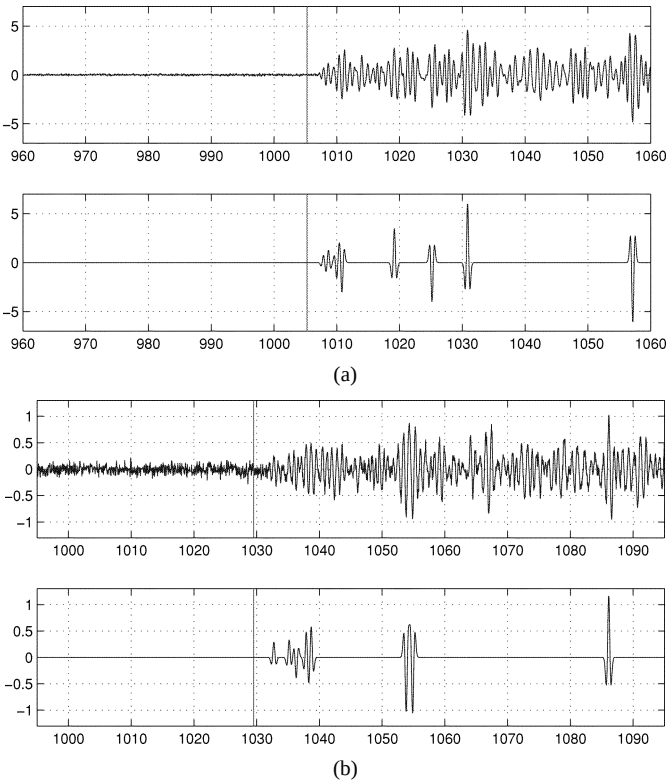

Fig. 6. ToA algorithm tested on measured signal at location 9 and 13. The vertical scale is in millivolts. Vertical line in each plot show the ToA of the direct path signal based on true measured range, assuming the presence of a clear LoS. $\theta_\delta = 100$ ns and θ_ρ was determined so that $P_{\mathrm{FA}} + P_{\mathrm{M}}$ is minimized. The values of θ_ρ used in each test are (a) 0.050 and (b) 0.154.

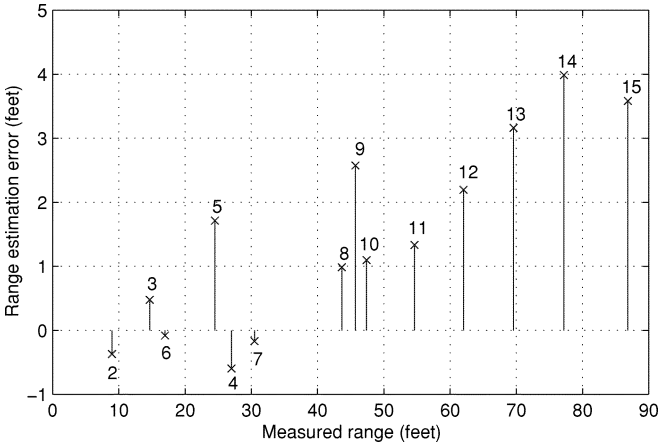

Fig. 7. Range estimation errors (estimated range–measured range). The numbers are the index of measurement positions. Ranging errors shown in this plot contains excessive propagation delay in the blockage structures.

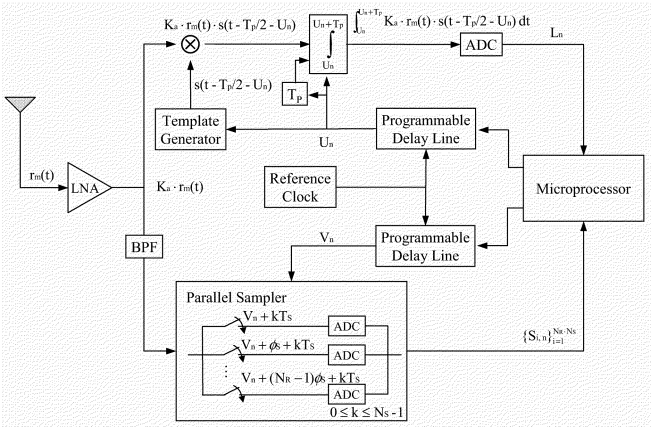

Fig. 8. Receiver schematic of UWB ranging system.

at long ranges, probably because the structure of LoS blockage was more complex at these locations.

VII. Design of UWB Ranging System

A. System Description

Withington *et al.* [7] introduced an UWB scanning receiver system which, using two correlators, has the capability of communication and channel pulse response measurement. The block diagram of an UWB ranging system using a correlator and a parallel sampler is shown in Fig. 8. When the signal is received, the correlator synchronizes with the signal, U_n being the time-tracking point in the nth time frame. Once the correlator is locked, the parallel sampler starts sampling the incoming signal under the time control of a trigger signal. The trigger time V_n in the nth time frame is controlled relative to the tracking time U_n. This parallel sampler is composed of a bank of N_{R} individual samplers and N_{R} analog-to-digital converters (ADC). Each individual sampler takes N_{S} samples per time frame at a sampling rate of $1/T_{\mathrm{S}}$ Hz. The offset in the sampling times of two adjacent individual samplers is ϕ_{s}, which satisfies

$$\phi_{\mathrm{s}} \cdot N_{\mathrm{R}} = T_{\mathrm{S}}. \tag{34}$$

Total $N_{\mathrm{S}} \cdot N_{\mathrm{R}}$ samples are taken in each time frame by this parallel sampler and the overall sampling frequency is $1/\phi_{\mathrm{s}}$ Hz. To acquire an acceptable SNR, each sample is integrated over several time frames. By changing the sampler's trigger time relative to the time-tracking point, the sampling frequency of the measured signal can be increased.

B. Two-Way Ranging Scheme

A UWB ranging system estimates the range by measuring signal round-trip time without a common timing reference. This ranging scheme uses a two-way remote synchronization technique [12] employed in satellite systems. Fig. 9 is the timing diagram of this approach. A pair of UWB radios are time multiplexed with a period of T_{M}. Each radio switches between a transmission mode and a reception mode every $T_{\mathrm{M}}/2$ s. Radio 1 transmits signal 1, which is a train of pulses without modulation. It is received by radio 2 and signal 1′ denotes the captured signal. The time-multiplex period T_{M} is assumed to be large

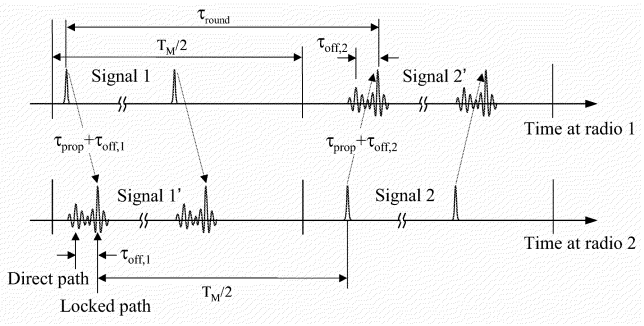

Fig. 9. Evaluation of the signal round-trip time.

enough relative to the temporal profile of the received signal so that it does not affect the next transmission. The delay between transmission and reception of this signal is $\tau_{\mathrm{prop}} + \tau_{\mathrm{off},1}$, where τ_{prop} is the propagation time, and $\tau_{\mathrm{off},1}$ represents the time offset between the locked path and the direct path. With a known delay of $T_{\mathrm{M}}/2$ from the front end of signal 1′, radio 2 transmits signal 2 and it is captured by radio 1. Signal 2′ denotes the captured signal by radio 1. Similarly, a delay of $\tau_{\mathrm{prop}} + \tau_{\mathrm{off},2}$ exists in this direction. The structures of signal 2 and signal 2′ are similar to those of signal 1 and signal 1′, respectively. Radio 1 can measure the signal round-trip time, τ_{round}, which is

$$\tau_{\mathrm{round}} \approx 2\tau_{\mathrm{prop}} + \frac{T_{\mathrm{M}}}{2} + \tau_{\mathrm{off},1} + \tau_{\mathrm{off},2}. \tag{35}$$

Then, the signal propagation time can be approximated by

$$\tau_{\mathrm{prop}} \approx \frac{\tau_{\mathrm{round}} - T_{\mathrm{M}}/2 - \tau_{\mathrm{off},1} - \tau_{\mathrm{off},2}}{2}. \tag{36}$$

Radio 2 informs radio 1 of $\tau_{\mathrm{off},1}$ afterwards with a few bits of information so that radio 1 can evaluate the signal propagation time. If the SNR of the measured signal is not large enough, the two radios increase the signal measurement time to acquire an acceptable SNR.

VIII. Conclusion

According to tests on the propagation data, there exists excessive propagation delay in the LoS blockage material which is considerable when the structure of this blockage is complex. This excessive propagation delay is a limiting factor in UWB ranging performance through materials.

Acknowledgment

The authors would like to thank Prof. K. Chugg and Prof. U. Mitra for their suggestions.

References

[1] R. A. Scholtz *et al.*, "UWB radio deployment challenges," in *Proc. Personal, Indoor Mobile Radio Communications (PIMRC 2000)*, vol. 1, 2000, pp. 620–625.

[2] M. Z. Win and R. A. Scholtz, "Energy capture versus correlator resources in ultra-wide bandwidth indoor wireless communications channels," in *Proc. Milcom*, vol. 3, Nov. 1997, pp. 1277–1281.

[3] ——, "Ultra-wide bandwidth signal propagation for indoor wireless communications," in *Proc. ICC*, June 1997.

[4] J. M. Cramer, R. A. Scholtz, and M. Z. Win, "Spatio–temporal diversity in ultra-wideband radio," in *Proc. WCNC*, vol. 2, 1999, pp. 888–892.

[5] J. M. Cramer, M. Z. Win, and R. A. Scholtz, "Evaluation of multipath characteristics of the impulse radio channel," in *Proc. PIMRC*, vol. 2, 1998, pp. 864–868.
[6] J. M. Cramer, R. A. Scholtz, and M. Z. Win, "Evaluation of an ultra-wideband propagation channel," *IEEE Trans. Antennas Propagat.*, vol. 50, pp. 561–570, May 2002.
[7] P. Withington, R. Reinhardt, and R. Stanley, "Preliminary results of an ultra-wideband (impulse) scanning receiver," in *Proc. MILCOM*, vol. 2, 1999, pp. 1186–1190.
[8] T. G. Manickam, R. J. Vaccaro, and D. W. Tufts, "A least-squares algorithm for multipath time-delay estimation," *IEEE Trans. Signal Processing*, vol. 42, pp. 3229–3233, Nov. 1994.
[9] I. Ziskind and M. Wax, "Maximum likelihood localization of multiple sources by alternating projection," *IEEE Trans. Acoust., Speech, Signal Processing*, vol. 36, pp. 1553–1560, Oct. 1988.
[10] H. G. Schantz and L. Fullerton, "The diamond dipole: A Gaussian impulse antenna," in *Proc. IEEE AP-S Int. Symp.*, Boston, MA, July 2001.
[11] J. R. Rice, "First-occurrence time of high-level crossings in a continuous random process," *J. Acoust. Soc. Amer.*, vol. 39, pp. 323–335, 1966.
[12] W. C. Lindsey and M. K. Simon, *Phase and Doppler Measurements in Two-Way Phase-Coherent Tracking Systems*. New York: Dover, 1991.
[13] E. L. Lehmann, *Nonparametrics: Statistical Methods Based on Ranks*. San Francisco, CA: McGraw-Hill, 1975.
[14] P. E. Greenwood and M. S. Nikulin, *A Guide to Chi-Squared Testing*. New York: Wiley, 1975.

Joon-Yong Lee was born in Seoul, Korea, in 1970. He received the B.S. degree in electrical engineering from Hong-Ik University, Seoul, Korea, in 1993, and the M.S. and Ph.D. degrees in electrical engineering from the University of Southern California (USC), Los Angeles, CA, in 1997 and 2002, respectively.

From 1998 to 2002, he was a Research Assistant with the Ultra-Wideband Radio Laboratory (UltraLab), USC. At USC, he worked primarily on the design of UWB ranging systems. His research interests are the characterization of UWB propagation channels and the design of UWB positioning systems. Since 2002, he has been with the School of Computer Science & Electrical Engineering, Handong Global University, Pohang, Korea, as a Faculty Member.

Robert A. Scholtz (S'56–M'59–SM'73–F'80–LF'02) was born in Lebanon, OH, on January 26, 1936. He is a Distinguished Alumnus of the University of Cincinnati, OH, where, as a Sheffield Scholar, he received the E.E. degree in 1958. He was a Hughes Masters and Doctoral Fellow while obtaining the M.S. and Ph.D. degrees in electrical engineering from University of Southern California (USC), Los Angeles, in 1960, and Stanford University, Stanford, CA, in 1964, respectively.

While working on missile radar signal processing problems, he remained part-time at Hughes Aircraft Company until 1978. In 1963, he joined the faculty of the USC, where he is now Professor of electrical engineering. From 1984 to 1989, he served as Director of USC's Communication Sciences Institute. He was Chairman of the Electrical Engineering Systems Department from 1994 to 2000. In 1996, as part of the Integrated Media Systems Center effort, he was instrumental in forming the Ultra-wideband Radio Laboratory (UltRa Lab) to provide facilities for the design and test of impulse radio systems and other novel high-bandwidth high-data-rate wireless mobile communication links. He has consulted for the LinCom Corporation, Axiomatix, Inc., the Jet Propulsion Laboratory, Technology Group, TRW, Pulson Communications (Time Domain Corporation), and Qualcomm, as well as various government agencies. His research interests include communication theory, synchronization, signal design, coding, adaptive processing, and pseudonoise generation, and their application to communications and radar systems. He co-authored *Spread Spectrum Communications* with M. K. Simon, J. K. Omura, and B. K. Levitt and *Basic Concepts in Information Theory and Coding* with S. W. Golomb and R. E. Peile. He has been General Chairman of five workshops in the area of communications, including most recently the Ultrawideband Radio Workshop held in May 1998, and has been an active participant on NSF panels and in research planning workshops of the U.S. Army Research Office.

Dr. Scholtz was elected to the grade of Fellow in the IEEE, "for contributions to the theory and design of synchronizable codes for communications and radar systems" in 1980. In 1983, he received the Leonard G. Abraham Prize Paper Award for the historical article, "The origins of spread spectrum communications;" this same paper received the 1984 Donald G. Fink Prize Award given by the IEEE. His paper "Acquisition of spread-spectrum signals by an adaptive array" with D. M. Dlugos received the 1992 Senior Award of the IEEE Signal Processing Society. His paper "Strategies for minimizing the intercept time in a mobile communication network with directive/adaptive antennas," with J.-H. Oh received the Ellersick Award for the best unclassified paper at Milcom 1997. His paper "ATM based ultrawide bandwidth (uwb) multiple-access radio network for multimedia PCS" with students M. Z. Win, J. H. Ju, X. Qiu, and colleague V. O. K. Li received the best student paper award from the NetWorld+Interop'97 program committee. In 2001, he received the Military Communications Conference Award for Technical Achievement. He has been an active member of the IEEE for many years, manning important organizational posts, including Finance Chairman for the 1977 National Telecommunications Conference, Program Chairman for the 1981 International Symposium on Information Theory, and Board of Governors positions for the Information Theory Group and the Communications Society.